

Article

Surface Modification of Bi₂O₃ Nanoparticles with Biotinylated β -Cyclodextrin as a Biocompatible Therapeutic Agent for Anticancer and Antimicrobial Applications

Jogy Alex and Thomas V. Mathew * 

Department of Chemistry, St. Thomas College Palai, Arunapuram P.O., Kottayam 686574, Kerala, India

* Correspondence: majothomas@stcp.ac.in or majothomas@gmail.com; Tel.: +91-9745180355

Abstract: Bismuth oxide nanoparticles with appropriate surface chemistry exhibit many interesting properties that can be utilized in a variety of applications. This paper describes a new route to the surface modification of bismuth oxide nanoparticles (Bi₂O₃ NPs) using functionalized beta-Cyclodextrin (β -CD) as a biocompatible system. The synthesis of Bi₂O₃ NP was done using PVA (poly vinyl alcohol) as the reductant and the Steglich esterification procedure for the functionalization of β -CD with biotin. Ultimately, the Bi₂O₃ NPs are modified using this functionalized β -CD system. The particle size of the synthesized Bi₂O₃ NPs is found to be in the range of 12–16 nm. The modified biocompatible systems were characterized using different characterization techniques such as Fourier transform infrared spectroscopy (FTIR), transmission electron microscopy (TEM), scanning electron microscopy (SEM), X-ray powder diffraction (XRD) and Differential Scanning Calorimetric analysis (DSC). Additionally, the antibacterial and anticancerous effects of the surface-modified Bi₂O₃ NP system were also investigated.

Keywords: bismuth oxide nanoparticles; beta-cyclodextrin; biotin; antibacterial; anticancerous studies



Citation: Alex, J.; Mathew, T.V. Surface Modification of Bi₂O₃ Nanoparticles with Biotinylated β -Cyclodextrin as a Biocompatible Therapeutic Agent for Anticancer and Antimicrobial Applications. *Molecules* **2023**, *28*, 3604. <https://doi.org/10.3390/molecules28083604>

Academic Editors: Sumiyyah Sabar, Lee D. Wilson and Ali H. Jawad

Received: 5 March 2023

Revised: 12 April 2023

Accepted: 15 April 2023

Published: 20 April 2023



Copyright: © 2023 by the authors. Licensee MDPI, Basel, Switzerland. This article is an open access article distributed under the terms and conditions of the Creative Commons Attribution (CC BY) license (<https://creativecommons.org/licenses/by/4.0/>).

1. Introduction

Inorganic nanoparticles (NPs) have achieved great significance in recent times for their potential to be used in biological and therapeutic applications [1–8]. The key characteristics of nanoparticles include (i) the high-level surface area to volume ratio of NPs which enables the inclusion of a high density of functional moieties [9], (ii) the distinctive physicochemical characteristics (electric, optical, and magnetic) resulting from the nanoscale scale [10], and (iii) NPs can interact with cells and biomolecules more effectively because of their similar size to biomacromolecules [11,12], and these can be explored to open the myriad possibilities ranging from therapeutic practices to space technologies [13,14]. There are some nanoparticles and their composites, although that is not as well known. This paper focuses on the Bi₂O₃ nanoparticles that belong to this category. These nanoparticles raised more and more interest in the scientific community due to their cost-effective manufacturing processes, high stability, and versatility in terms of their size and shape. Moreover, the high atomic number of bismuth brings about high energy radiation attenuation greater than that of lead, making it at negligible risk of toxicity. Bismuth oxide has high dielectric permittivity, good refractive index, photoconductivity, and photoluminescence [15]. Thus, it has potential uses in a variety of fields, including solid-state fuel cells [16], photovoltaic cells [17], high-temperature superconductors [18], photocatalysts [19], gas sensors [20], optical coatings [21], and biomedical applications [22]. The five crystallographic polymorphs of Bi₂O₃ are α -Bi₂O₃ (monoclinic), β -Bi₂O₃ (tetragonal), γ -Bi₂O₃ (body-centered cubic), δ -Bi₂O₃ (cubic), and ϵ -Bi₂O₃ (triclinic). α -Bi₂O₃ at ambient temperature and δ -Bi₂O₃ at high temperatures are stable, whereas the remaining four are metastable phases [23]. The

synthesis of Bi_2O_3 NPs can be done through various methods such as chemical vapour deposition (CVD) [24], precipitation method [25], electrodeposition [26], microwave-assisted synthesis [27], microemulsion method [28], sol-gel methods [29], hydrothermal synthesis [30] and so on. The aggregation behaviour of the metal oxide nanoparticles limits its application and the only solution to reduce this is to modify the surface of the nanoparticles. The surface modification of the synthesized Bi_2O_3 NPs should be performed for improving the dispersion, surface activity, and biocompatibility of Bi_2O_3 NPs, thereby enhancing their physicochemical properties [31]. Herein, we make use of functionalized β -cyclodextrin for the surface modification of Bi_2O_3 NPs.

β -cyclodextrin (β -CD), a cyclic oligosaccharide, possesses a molecular structure that has a hydrophobic core chamber and a hydrophilic outside [32]. Based on chemical processes, a variety of substances may be “grabbed” by the cyclodextrin cavity to create inclusion complexes [33]. There have been reports of nanoparticles’ agglomeration being prevented, and their colloidal and thermal stability being increased, by grafting a cyclodextrin polymer onto them [34,35]. The ability to do this has led to the widespread usage of CDs in a variety of fields, including catalysis, pharmaceutical science, separation technology, and many others [36–39]. For the modification of β -cyclodextrin, biotin, a water-soluble vitamin, can be used. Biotin has special functions in chromatin structure, epigenetic gene control, and cell signaling [40].

Accordingly, the present work is directed towards an efficient method for the surface modification of Bi_2O_3 NP using biotinylated β -cyclodextrin. We described the experimental detail for the preparation of Bi_2O_3 NPs using PVA (poly vinyl alcohol) as the reductant, in order to obtain the NPs with small particle size and size distribution that is needed for biomedical application. The developed biocompatible system was characterized by UV-Vis, FT-IR, XRD, SEM, and TEM. The antibacterial and anticancerous activity of the surface-modified system was also evaluated. The zeta potential of beta-CD, bismuth nanoparticles, and bismuth nanoparticles with biotinylated beta-CD was determined by the dynamic light scattering (DLS) method.

2. Results and Discussion

2.1. Characterization of Bi_2O_3 NPs

FTIR spectrum of Bi_2O_3 gave the following data: 1380 cm^{-1} and 2352 cm^{-1} : $\nu_{\text{C-O}}$ (vibr), 421 , 540 and 844 cm^{-1} : $\nu_{\text{Bi-O}}$ (vibr) (Figure 1a). The XRD pattern of Bi_2O_3 nanoparticles shows strong and sharp peaks, indicating that the synthesized nanoparticles are in the crystals phase as represented in Figure 1b. The peaks are in support of the monoclinic crystals phase of Bi_2O_3 based on COD No. 96-152-6459 at the 2θ value of 23.91° , 27.27° , 30.22° , 32.90° , 38.07° , 39.74° , 48.82° , 56.16° , and 64.63° which are associated with the planes (102), (120), (012), (121), (131), (122), (113), (222), and (104). The crystallite size of Bi_2O_3 NPs is calculated by the Debye Scherrer equation and obtained in the range of 12–16 nm. Figure 1c is the UV-Vis DRS spectrum of Bi_2O_3 NPs which also confirms the formation of Bi_2O_3 NPs by exhibiting absorption peaks at 283 nm and 268 nm.

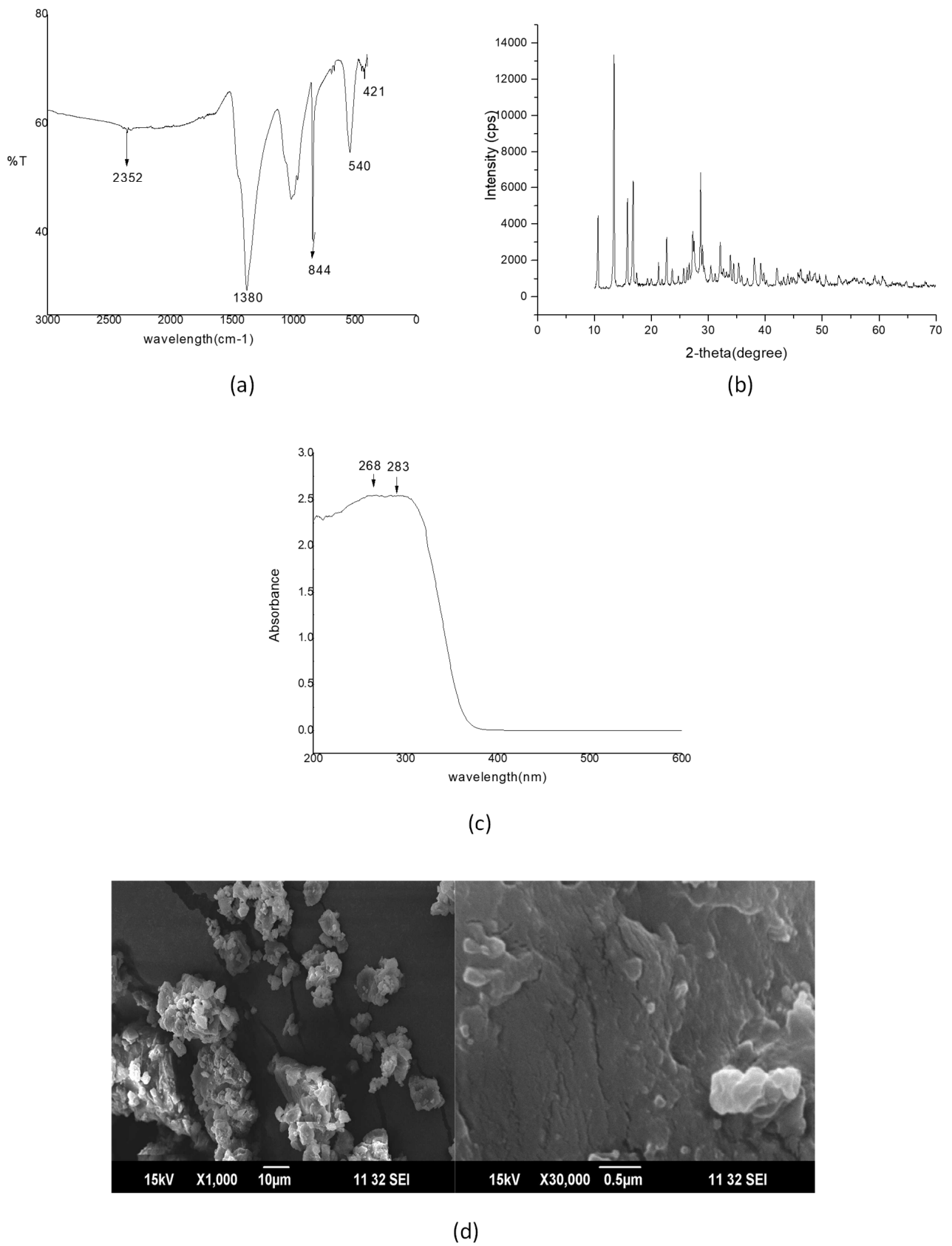


Figure 1. Cont.

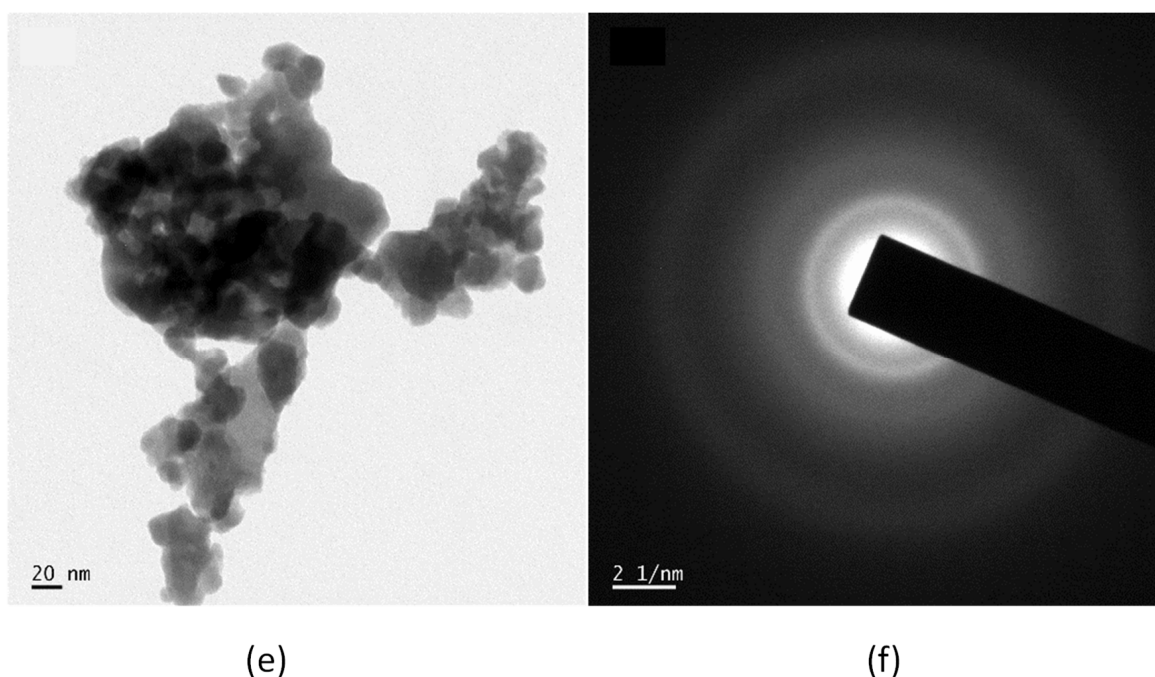


Figure 1. (a) FTIR of Bi_2O_3 NPs, (b) XRD pattern of Bi_2O_3 NPs, (c) UV-Vis DRS spectrum of Bi_2O_3 NPs, (d) SEM images of Bi_2O_3 NPs under different magnification, (e) TEM images of Bi_2O_3 NP and (f) SAED patterns of Bi_2O_3 NP.

The SEM gives information about the surface morphologies and particle sizes of the prepared Bi_2O_3 sample. The SEM images of Bi_2O_3 under different magnifications are presented in Figure 1d. The Bi_2O_3 NP has a spherical shape in morphology with an average diameter of 12–16 nm.

Figure 1e depicts the TEM image of Bi_2O_3 NPs, and it is clear that the synthesized monoclinic Bi_2O_3 NPs possess a spherical shape with a crystalline diameter in the range of 12–16 nm. The Selected Area Electron Diffraction (SAED) patterns of Bi_2O_3 NPs are shown in Figure 1f and the ring diffractogram agreed with the crystalline structure of monoclinic Bi_2O_3 NPs. Each ring's diameter reflects the interplanar distance of a plane system that is present in the sample. The particle size obtained by TEM analysis was highly consistent with that obtained using XRD analysis.

2.2. Characterization of the Surface-Modified Bi_2O_3 Nanoparticles Using Biotinylated β -Cyclodextrin

The FT-IR spectrum of the BiONP- β -CD-Biotin system gave the following data (Figure 2a): 3295 cm^{-1} : $\nu_{\text{O-H}}$ (str) of β -CD, 2922 cm^{-1} : $\nu_{\text{C-H}}$ (aliph, str) of CH_2 , 1722 cm^{-1} : $\nu_{\text{C=O}}$ (str) of COOR, 1624 cm^{-1} : $\nu_{\text{C=C}}$ (aliph, str), 1255 cm^{-1} : $\nu_{\text{C-H}}$ (overtone, str) of biotin, 1481 cm^{-1} : $\nu_{\text{C-H}}$ (str) of biotin, 1020 cm^{-1} : $\nu_{\text{C-O}}$ (str) of biotin, 423 cm^{-1} , 566 cm^{-1} and 851 cm^{-1} : $\nu_{\text{Bi-O}}$ (vibr). The basic nature and size of the surface-modified Bi_2O_3 nanoparticles using biotinylated β -cyclodextrin were interpreted based on the XRD analysis and are shown in Figure 2b. The peaks are in support of the fact that the monoclinic crystals phase of Bi_2O_3 is conserved in the final surface-modified system and the 2θ values obtained are in association with the planes (102), (120), (012), (121), (131), (122), (113), (222), and (104). The low-intensity peaks which are obtained below 30° are due to the β -CD in the final surface-modified system.

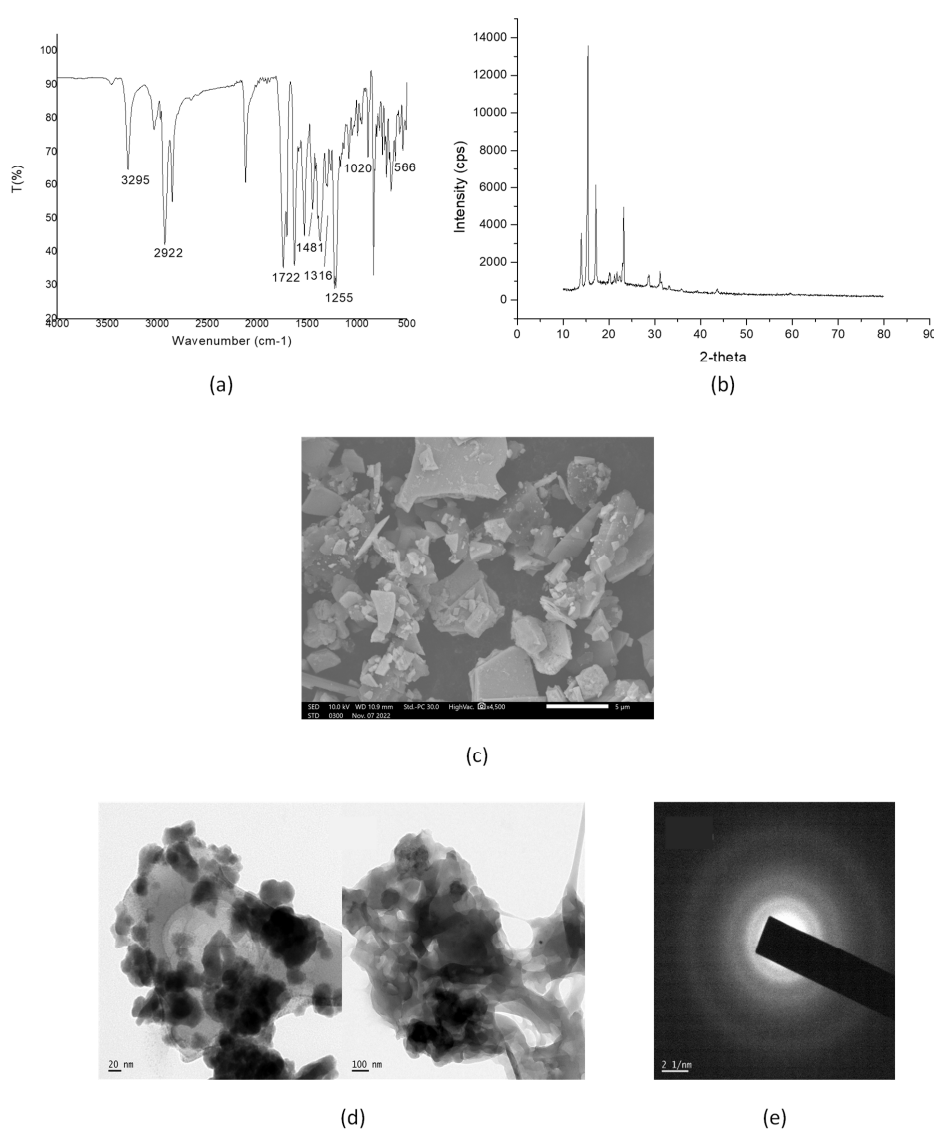


Figure 2. (a) FTIR spectrum of the surface-modified Bi_2O_3 nanoparticles using biotinylated β -cyclodextrin, (b) XRD pattern of the surface-modified Bi_2O_3 nanoparticles using biotinylated β -cyclodextrin, (c) SEM image of the surface-modified Bi_2O_3 nanoparticles using biotinylated β -cyclodextrin, (d) TEM images of the surface-modified Bi_2O_3 nanoparticles using biotinylated β -cyclodextrin, and (e) SAED image of the surface-modified Bi_2O_3 nanoparticles using biotinylated β -cyclodextrin.

Using SEM, surface morphology studies of the functionalized β -CD system on the surface-modified Bi_2O_3 NPs were carried out in Figure 2c. The surface-modified Bi_2O_3 NPs with the functionalized β -CD system were found to have a well-dispersed morphology. Figure 2d displays transmission electron microscope (TEM) and Figure 2e the SAED images of surface-modified Bi_2O_3 NPs with the functionalized β -CD system, which shows that the particle in the surface-modified product retains its original shape, surface morphology, and particle size.

2.3. Antimicrobial Studies

The gram-positive bacterial strains (*S. pneumoniae* and *S. aureus*) and two gram-negative (*P. aeruginosa* and *K. pneumoniae*) strains were used to analyse the bacterial resistance by the agar diffusion test. Measurements were done five times for each strain. In all tests, the control did not achieve an inhibition zone. The diameter of the zone of inhibition for each bacterial strain was determined from the mean value of five replicates.

Results are represented as the mean of five replicates \pm standard deviation (Table 1). The average diameter of inhibition zones for surface-modified Bi_2O_3 NPs against *S. pneumoniae*, *S. aureus*, *P. aeruginosa*, and *K. pneumoniae* are 14.26 mm Figure 3a, 17.54 mm Figure 3b, 15.31 mm, Figure 3c, and 12.23 mm Figure 3d, respectively.

Table 1. Result of the diameter of the inhibition zone observed for BiONP- β -CD-Biotin system against bacteria.

Bacterial Strain Tested	Inhibition Zone (mm) \pm Standard Deviation Observed for BiONP- β -CD-Biotin System
<i>S. pneumoniae</i>	14.26 \pm 0.53
<i>S. aureus</i>	17.54 \pm 0.21
<i>P. aeruginosa</i>	15.31 \pm 0.36
<i>K. pneumoniae</i>	12.23 \pm 0.24

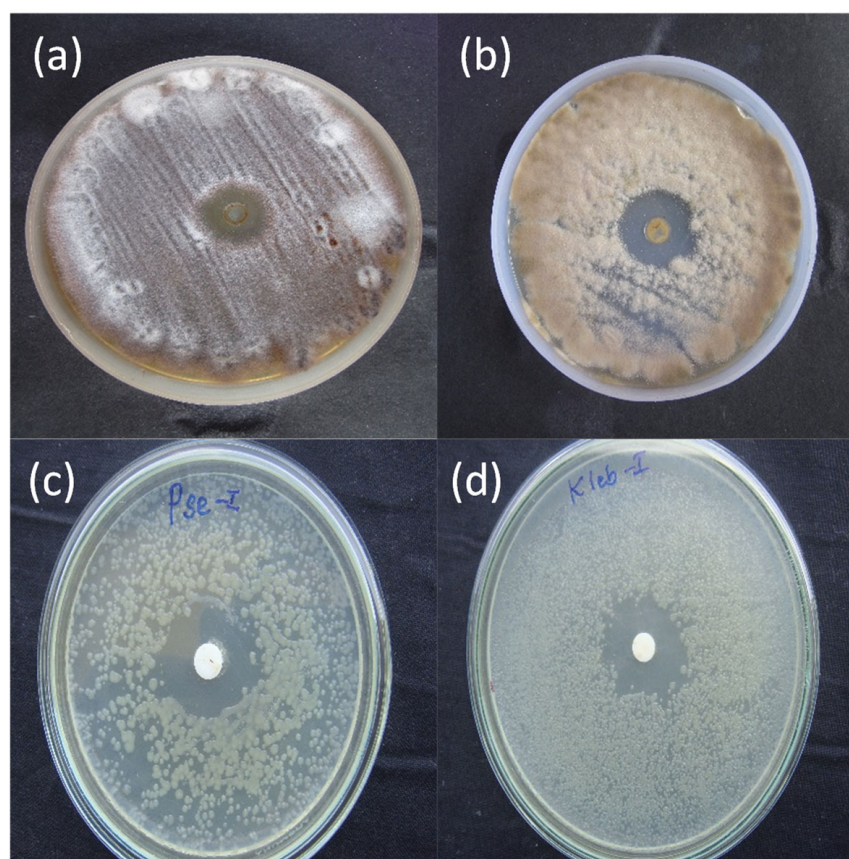


Figure 3. Inhibition zone obtained for BiONP- β -CD-Biotin system against bacteria (a) *S. pneumoniae* (b) *S. aureus* (c) *P. aeruginosa* and (d) *K. pneumoniae*.

2.4. In Vitro Cytotoxicity Studies

In vitro cytotoxicity of three different cancer cell lines; Hep G2, MCF-7, and A549 were evaluated using MTT assays and the results were illustrated as a graphical plot in Figure 4 and Table 2. For this purpose, the cancer cell lines were exposed to the BiONP- β -CD-Biotin system at various concentrations (6.25, 12.5, 25, 50, and 100 $\mu\text{g}/\text{mL}$) for 24 h. In all three cases, the cell viability declined with a rise in the concentration of the surface-modified Bi_2O_3 NPs with biotinylated β -cyclodextrin. The IC_{50} value of surface-modified Bi_2O_3 NPs with biotinylated β -cyclodextrin reported against Hep G2, MCF-7, and A549 cell lines are 76.743, 62.336, and 67.363 $\mu\text{g}/\text{mL}$ respectively and it was determined using ED50 PLUS V1.0

Software. All studies were conducted in triplicate, with results expressed as Mean \pm SE. A one-way analysis of variance (ANOVA) and Dunnett's test were used to analyse the results. $p < 0.001$ in comparison to the control group was statistically significant.

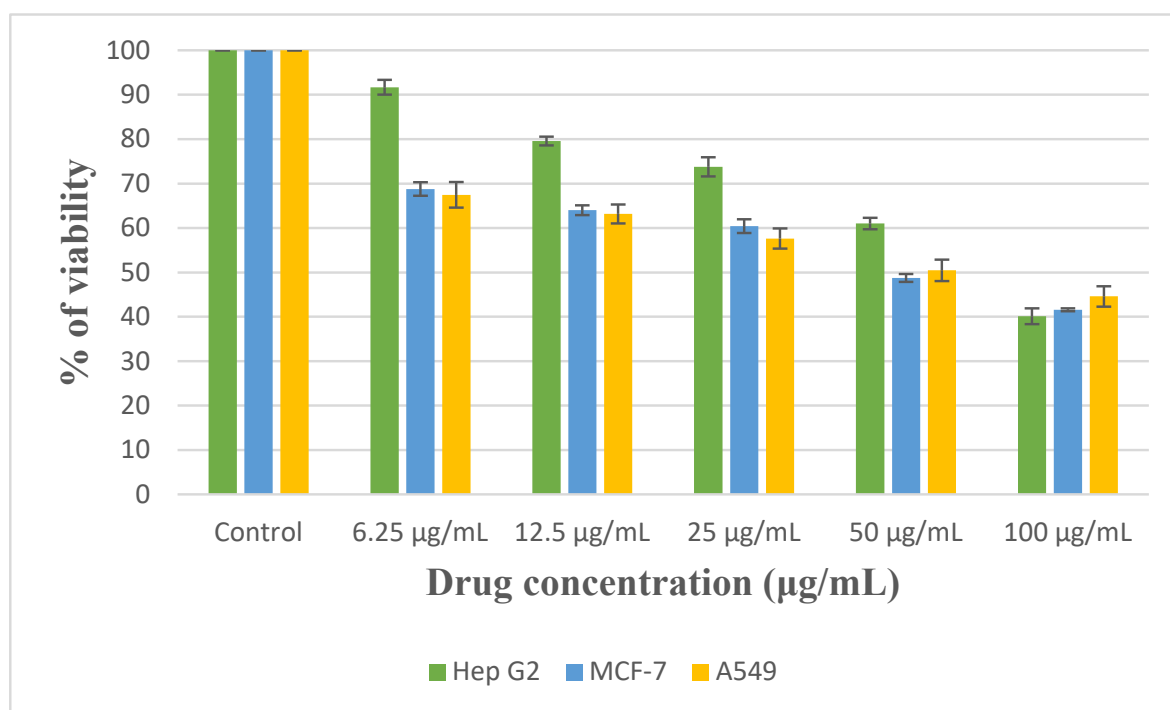


Figure 4. Graphical plot of in vitro cytotoxicity of the BiONP-β-CD-Biotin system against Hep G2, MCF-7, and A549.

Table 2. In vitro cytotoxicity of the BiONP-β-CD-Biotin system against Hep G2, MCF-7, and A549.

Hep G2 Cancer Cell Lines					
Drug Concentration	6.25	12.5	25	50	100
Percentage of cell viability	91.69 ± 0.55	79.58 ± 0.32	73.78 ± 0.72	61.00 ± 0.43	40.11 ± 0.60
MCF-7 cancer cell lines					
Drug Concentration	6.25	12.5	25	50	100
Percentage of cell viability	68.78 ± 0.51	63.99 ± 0.36	60.42 ± 0.52	48.76 ± 0.30	41.57 ± 0.12
A549 cancer cell lines					
Drug Concentration	6.25	12.5	25	50	100
Percentage of cell viability	67.45 ± 0.97	63.14 ± 0.72	57.62 ± 0.76	50.46 ± 0.81	44.58 ± 0.77

2.5. Thermal Studies

The relationship between the temperature change and mass loss is expressed using DSC (Differential Scanning Calorimetry) and the DSC plot of the surface-modified Bi₂O₃ NP system is shown in Figure 5 [41–43]. On increasing the temperature from room temperature, in the DSC plot, an endothermic peak was observed where the onset temperature, the peak temperature, and the end set temperature are at 54.22 °C, 78.19 °C, and 104.23 °C, respectively. The corresponding area under the curve is 1393.97 mJ and the ΔH value, 139.39 J/g, is responsible for the formation of more thermally stable products.

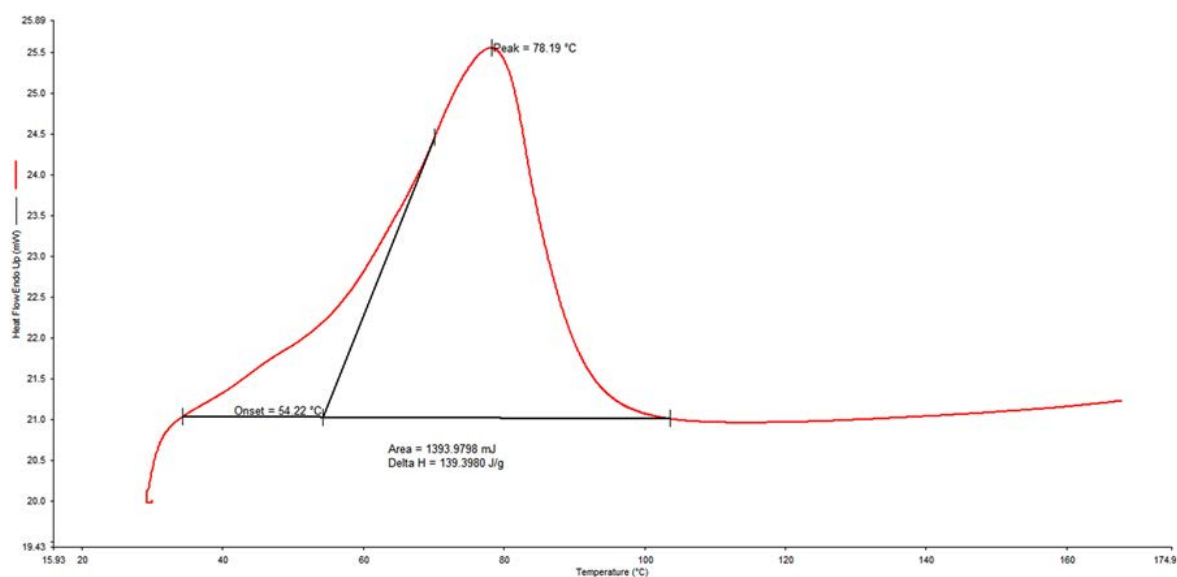


Figure 5. DSC plot of the surface-modified Bi₂O₃ NPs using β -CD functionalized with biotin.

2.6. Zeta Potential Analysis

The zeta potential of beta-CD, bismuth oxide nanoparticles, and bismuth oxide nanoparticles with biotinylated beta-CD was determined by the dynamic light scattering (DLS) method using a nanoparticle analyser (Horiba, nanopartica SZ 100). The zeta potential of beta-CD, Bi₂O₃ NPs, and Bi₂O₃ NPs with biotinylated beta-CD was obtained as -26.30 mV, 45.10 mV, and 41.20 mV respectively (Figure 6). The value of ± 30 mV is normally used to assume the stability of NPs; Zeta potential values more than +30 mV and less than -30 mV represent stable conditions, but values between -30 mV and +30 mV show unstable conditions [44]. Zeta potential is thus indicative of the probable physical stability of a formulation [45]. The positive zeta potential value of bismuth nanoparticles with biotinylated beta-CD was due to the presence of biotin and bismuth nanoparticles. The reduction in the zeta potential value of bismuth nanoparticles with biotinylated beta-CD compared to that of bismuth was due to the effective grafting of negatively charged beta-cyclodextrin molecules on the surface of biotinylated bismuth nanoparticles.

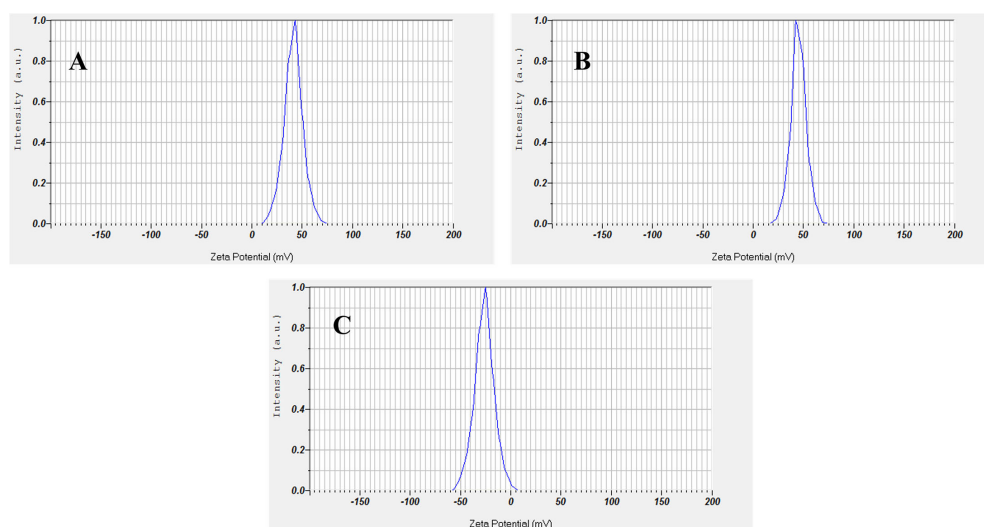


Figure 6. The zeta potential of (A) beta-CD, (B) bismuth oxide nanoparticles, and (C) bismuth oxide nanoparticles with biotinylated beta-CD.

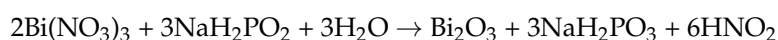
3. Experimental

3.1. Materials and Methods

Bismuth nitrate alkaline $\text{Bi}_5\text{O}(\text{OH})_9(\text{NO}_3)_4$ was used as a precursor. All of the chemicals and solvents used in the investigation were of analytical grade. Sodium-hypophosphite ($\text{NaH}_2\text{PO}_2 \cdot \text{H}_2\text{O}$), sodium hydroxide (NaOH), nitric acid (HNO_3), poly vinyl alcohol (PVA), ethanol, biotin, cyclodextrin, and DMSO are purchased from Nice chemicals. UV-Vis spectra were captured using a Shimadzu UV-visible NIR spectrophotometer (Shimadzu Corporation, Koyoto, Japan) operating between 190 and 1100 nm, and X-ray diffraction (XRD) measurements were performed using a Rigaku Miniflex-600 X-ray diffractometer with $\text{CuK}\alpha$ radiation in a θ - 2θ configuration. The FT-IR spectra were captured using a Shimadzu-400 spectrophotometer with a scanning range of 4000 – 400 cm^{-1} . A HITACHI S-4200 scanning electron microscope operating at 20 kV and a JEOL JEM-2100 transmission electron microscope (TEM) were utilized to examine the morphology and size of the Bi_2O_3 NPs and surface-modified products. The zeta potential of beta-CD, bismuth nanoparticles, and bismuth nanoparticles with biotinylated beta-CD was determined by the dynamic light scattering (DLS) method using a nanoparticle analyser (Horiba, nanopartica SZ 100, Horiba Ltd., Minami-ku, Koyoto, Japan).

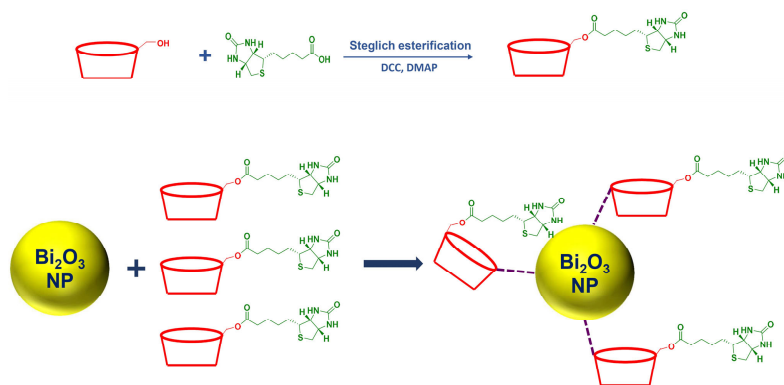
3.2. Synthesis of Bi_2O_3 NPs

Initially, 0.052 g of PVA and 5 mL of 1 M $\text{Bi}(\text{NO}_3)_3$ were dissolved in concentrated nitric acid and 5 mL of water was added to the beaker at room temperature. Then, 40 mL of 5 M $\text{NaH}_2\text{PO}_2 \cdot \text{H}_2\text{O}$ was added. Dropwise additions of 0.52 g of NaOH in 70 mL are added to the solution until the pH reaches 2.5, followed by 20 min of stirring at room temperature. After transferring the beaker to an 80°C temperature-controlled oil bath, stirring continued for an additional one hour and thirty minutes. After the reaction was complete, the black precipitate was filtered and repeatedly washed with distilled water and ethanol to eliminate contaminations and byproducts.



3.3. Synthesis of Surface-Modified Bi_2O_3 Nanoparticles Using Biotinylated β -Cyclodextrin

By esterifying the $-\text{OH}$ group of β -CD with the $-\text{COOH}$ group of biotin by DCC coupling, β -cyclodextrin was made to be biotinylated (Steglich esterification). To obtain biotinylated β -CD surface modified Bi_2O_3 NP, about 1 gm of biotinylated β -CD and 0.25 gm of Bi_2O_3 NP were dispersed in 10 mL chloroform separately. Both solutions were mixed and stirred continuously for 3 h. After the stirring, the solution was allowed to dry and the obtained powder is the biotinylated β -CD modified bismuth oxide nanoparticle. Scheme 1 schematically depicts the methods involved in creating surface-modified Bi_2O_3 nanoparticles using biotinylated β -cyclodextrin.



Scheme 1. Graphical illustration of the surface-modified Bi_2O_3 nanoparticles with biotinylated β -cyclodextrin (BiONP- β -CD-Biotin).

3.4. Antimicrobial Activity

The antibacterial activity of the surface-modified system is evaluated by applying the agar well diffusion method. The antimicrobial activity of the BiONP- β -CD-Biotin system was evaluated against two gram-positive (*Streptococcus pneumoniae* and *Staphylococcus aureus*) and two gram-negative (*Pseudomonas aeruginosa* and *Klebsiella pneumoniae*) bacterial strains. To inoculate the agar, a volume of the microbial inoculum is dispersed throughout its whole surface. Then, a volume of extract solution (20–100 μ L) is injected into the well by creating a hole using a sterile cork borer. The test bacterial strain is then placed on it and the incubation procedure is repeated. The antimicrobial substance inhibits the growth of the tested microbial strain as it diffuses throughout the agar media. The diameters of the growth inhibition zones are then measured.

3.5. In Vitro Cytotoxicity Assays—MTT Assay

For cytotoxicity studies of chemicals and drug screening, in vitro cell viability and cytotoxicity studies with cultivated cells are often performed [46]. Currently, these tests are utilized in cancer research to evaluate the cytotoxicity and growth inhibition of possible cancer treatment candidates. In cell viability and cytotoxicity research, numerous cell activities, such as cell membrane permeability, ATP synthesis, cell adhesion, coenzyme creation, enzyme activity, and nucleotide absorption activity are measured [47]. MTT (3-(4,5-dimethylthiazol-2-yl)-2-5-diphenyltetrazolium bromide) assay is the most widely used colorimetric method for assessing cytotoxicity or cell viability [48]. By evaluating the activity of mitochondrial enzymes such as succinate dehydrogenase, this assay primarily analyses cell viability by measuring the efficiency with which cells carry out the mitochondrial function [49]. NADH transforms MTT into a purple formazan for this assay. Light absorbance at a particular wavelength can be used to calculate the amount of this product. The MTT method is widely used because it is simple to use, safe, and well-reproducible. In the present work, in vitro cytotoxicity of the BiONP- β -CD-Biotin system was assessed against cancer cell lines; Hep G2 (Human liver cancer), MCF-7 (Human breast cancer), and A549 (Human lung cancer). The study was conducted at the Center for Research on Molecular and Applied Sciences Pvt Ltd., Biogenix, DNRA 41, Thiruvananthapuram, Kerala, India. The cancer cell lines were cultured in a 25 cm² tissue culture flask containing DMEM supplemented with 10% FBS, L-glutamine, sodium bicarbonate, and an antibiotic solution containing Penicillin (100 U/mL), Streptomycin (100 μ g/mL), and Amphotericin B (2.5 μ g/mL). In a humidified, 5% CO₂ incubator, cell lines were maintained at 37 °C. A 96-well tissue culture plate, 5 \times 10³ cells/well were sown and cultured at 37 °C in a humidified 5% CO₂ incubator. After 24 h, the growth medium was removed, surface modified Bi₂O₃ NPs with biotinylated β -cyclodextrin in DMEM were five times serially diluted by two-fold dilution (100 μ g, 50 μ g, 25 μ g, 12.5 μ g, 6.25 μ g in 500 μ L of DMEM), and each concentration of 100 μ L was added in triplicates to the respective wells and incubated at 37 °C in a humidified 5% CO₂ incubator. Non-treated control cells were also maintained. After 24 h of incubation, the sample content was withdrawn from the wells and 30 μ L of reconstituted MTT solution was added to all test and cell control wells. The plate was then gently shaken and incubated at 37 °C in a humidified 5% CO₂ incubator for four hours. After the incubation period, the supernatant was removed, 100 μ L of MTT solubilization solution was added, and the wells were pipetted up and down gently to dissolve the formazan crystals. At a wavelength of 540 nm, absorbance values were measured using a microplate reader. Using the formula, the percentage of growth inhibition was computed:

$$\% \text{ of viability} = \frac{\text{Mean OD samples}}{\text{Mean OD of control groups}} \times 100$$

All studies were conducted in triplicate, with results expressed as Mean \pm SE. A one-way analysis of variance (ANOVA) and Dunnett's test were used to analyse the results. $p < 0.001$ in comparison to the control group was statistically significant.

4. Conclusions

Recently, the surface modification of metal oxide nanoparticles arises as a new class in nanotechnology with wide applications. Upon surface modification, the nanoparticles become stabilized against agglomeration and this type of modification also renders them compatible with another phase. In this article, we prepared Bi₂O₃ NPs with modified surfaces using the functionalized β -CD system, a system that is completely biocompatible. Using XRD, FT-IR, UV-Vis, TEM, and SEM respectively, all the acquired products were characterised. The thermal events that occurred in the final product were carried out using DSC. In this work, we also investigated the antibacterial and anticancerous influence of the BiONP- β -CD-Biotin system using the bacterial strains *S. pneumoniae*, *S. aureus*, *P. aeruginosa*, and *K. pneumonia*, and the cancerous cells Hep G2, MCF-7, and A549. The zeta potential of beta-CD, bismuth nanoparticles, and bismuth nanoparticles with biotinylated beta-CD was determined by the dynamic light scattering (DLS) method, which is indicative of the probable physical stability of the BiONP- β -CD-Biotin system.

Author Contributions: Conceptualization, T.V.M.; methodology, J.A. and T.V.M.; software, T.V.M.; validation, J.A. and T.V.M.; formal analysis, J.A.; investigation, J.A.; resources, J.A. and T.V.M.; data curation, J.A.; writing-original draft preparation, J.A.; writing-review and editing, T.V.M.; supervision, T.V.M.; project administration, J.A.; funding acquisition J.A. and T.V.M. All authors have read and agreed to the published version of the manuscript.

Funding: This research received no external funding.

Institutional Review Board Statement: Not applicable.

Informed Consent Statement: Not applicable.

Data Availability Statement: All relevant data are included in the article.

Conflicts of Interest: The authors declare no conflict of interest.

Sample Availability: Samples of the compounds are not available from the authors.

References

1. Zarschler, K.; Rocks, L.; Licciardello, N.; Boselli, L.; Polo, E.; Garcia, K.P.; De Cola, L.; Stephan, H.; Dawson, K.A. Ultrasmall Inorganic Nanoparticles: State-of-the-Art and Perspectives for Biomedical Applications. *Nanomed. Nanotechnol. Biol. Med.* **2016**, *12*, 1663–1701. [[CrossRef](#)] [[PubMed](#)]
2. Matsuura, K. Construction of Functional Biomaterials by Biomolecular Self-Assembly. *Bull. Chem. Soc. Jpn.* **2017**, *90*, 873–884. [[CrossRef](#)]
3. Kim, D.; Kim, J.; Park, Y.I.; Lee, N.; Hyeon, T. Recent Development of Inorganic Nanoparticles for Biomedical Imaging. *ACS Cent. Sci.* **2018**, *4*, 324–336. [[CrossRef](#)]
4. Diana, E.J.; Mathew, T. V Synthesis and Characterization of Surface-Modified Ultrafine Titanium Dioxide Nanoparticles with an Antioxidant Functionalized Biopolymer as a Therapeutic Agent: Anticancer and Antimicrobial Evaluation. *Colloids Surf. B Biointerfaces* **2022**, *220*, 112949. [[CrossRef](#)]
5. Jiao, M.; Zhang, P.; Meng, J.; Li, Y.; Liu, C.; Luo, X.; Gao, M. Recent Advancements in Biocompatible Inorganic Nanoparticles towards Biomedical Applications. *Biomater. Sci.* **2018**, *6*, 726–745. [[CrossRef](#)] [[PubMed](#)]
6. Kanchana, U.S.; Mathew, T.V. Surface Functionalization of ZnO Nanoparticles with Functionalized Bovine Serum Albumin as a Biocompatible Photochemical and Antimicrobial Agent. *Surf. Interfaces* **2021**, *24*, 101056. [[CrossRef](#)]
7. Bordbar-Khiabani, A.; Bahrampour, S.; Mozafari, M.; Gasik, M. Surface Functionalization of Anodized Tantalum with Mn₃O₄ Nanoparticles for Effective Corrosion Protection in Simulated Inflammatory Condition. *Ceram. Int.* **2022**, *48*, 3148–3156. [[CrossRef](#)]
8. Bordbar-Khiabani, A.; Yarmand, B.; Mozafari, M. Enhanced Corrosion Resistance and In-Vitro Biodegradation of Plasma Electrolytic Oxidation Coatings Prepared on AZ91 Mg Alloy Using ZnO Nanoparticles-Incorporated Electrolyte. *Surf. Coat. Technol.* **2019**, *360*, 153–171. [[CrossRef](#)]
9. Shang, L.; Nienhaus, K.; Nienhaus, G.U. Engineered Nanoparticles Interacting with Cells: Size Matters. *J. Nanobiotechnol.* **2014**, *12*, 5. [[CrossRef](#)]
10. Khan, I.; Saeed, K.; Khan, I. Nanoparticles: Properties, Applications and Toxicities. *Arab. J. Chem.* **2019**, *12*, 908–931. [[CrossRef](#)]
11. Din, F.U.; Aman, W.; Ullah, I.; Qureshi, O.S.; Mustapha, O.; Shafique, S.; Zeb, A. Effective Use of Nanocarriers as Drug Delivery Systems for the Treatment of Selected Tumors. *Int. J. Nanomed.* **2017**, *12*, 7291–7309. [[CrossRef](#)] [[PubMed](#)]
12. Mathew, T.V.; Kuriakose, S. Synthesis and Characterization of Sodium-Lithium Niobate Ceramic Structures and Their Composites with Biopolymers. *J. Adv. Ceram.* **2013**, *2*, 11–20. [[CrossRef](#)]

13. Mathew, T.V.; Kuriakose, S. 4-(1-Pyrenyl)Butyric Acid-Functionalised Chitosan as a Matrix for AgNP: Photoresponsive and Thermal Properties. *J. Polym. Res.* **2013**, *20*, 291. [[CrossRef](#)]
14. Yang, C.; Liu, G.; Chen, J.; Zeng, B.; Shen, T.; Qiu, D.; Huang, C.; Li, L.; Chen, D.; Chen, J.; et al. Chitosan and Polyhexamethylene Guanidine Dual-Functionalized Cotton Gauze as a Versatile Bandage for the Management of Chronic Wounds. *Carbohydr. Polym.* **2022**, *282*, 119130. [[CrossRef](#)]
15. Leontie, L.; Caraman, M.; Alexe, M.; Harnagea, C. Structural and Optical Characteristics of Bismuth Oxide Thin Films. *Surf. Sci.* **2002**, *507–510*, 480–485. [[CrossRef](#)]
16. Azad, A.M.; Larose, S.; Akbar, S.A. Bismuth Oxide-Based Solid Electrolytes for Fuel Cells. *J. Mater. Sci.* **1994**, *29*, 4135–4151. [[CrossRef](#)]
17. Mahmoud, W.E.; Al-Ghamdi, A.A. Synthesis and Properties of Bismuth Oxide Nanoshell Coated Polyaniline Nanoparticles for Promising Photovoltaic Properties. *Polym. Adv. Technol.* **2011**, *22*, 877–881. [[CrossRef](#)]
18. Sergeev, A.; Golev, I. High-Temperature Superconducting Materials Based on Bismuth with a Low Critical Current. *Mater. Today Proc.* **2019**, *11*, 489–493. [[CrossRef](#)]
19. Reverberi, A.P.; Varbanov, P.S.; Vocciante, M.; Fabiano, B. Bismuth Oxide-Related Photocatalysts in Green Nanotechnology: A Critical Analysis. *Front. Chem. Sci. Eng.* **2018**, *12*, 878–892. [[CrossRef](#)]
20. Bhande, S.S.; Mane, R.S.; Ghule, A.V.; Han, S.H. A Bismuth Oxide Nanoplate-Based Carbon Dioxide Gas Sensor. *Scr. Mater.* **2011**, *12*, 1081–1084. [[CrossRef](#)]
21. Fruth, V.; Popa, M.; Berger, D.; Ramer, R.; Gartner, M.; Ciulei, A.; Zaharescu, M. Deposition and Characterisation of Bismuth Oxide Thin Films. *J. Eur. Ceram. Soc.* **2005**, *25*, 2171–2174. [[CrossRef](#)]
22. Bartoli, M.; Jagdale, P.; Tagliaferro, A. A Short Review on Biomedical Applications of Nanostructured Bismuth Oxide and Related Nanomaterials. *Materials* **2020**, *13*, 5234. [[CrossRef](#)] [[PubMed](#)]
23. Kumar Trivedi, M.; Mohan Tallapragada, R.; Branton, A.; Trivedi, D.; Nayak, G.; Latiyal, O.; Jana, S. Evaluation of Atomic, Physical, and Thermal Properties of Bismuth Oxide Powder: An Impact of Biofield Energy Treatment. *Am. J. Nano Res. Appl.* **2015**, *2015*, 94–98.
24. Kim, H.W.; Myung, J.H.; Shim, S.H. One-Dimensional Structures of Bi₂O₃ Synthesized via Metalorganic Chemical Vapor Deposition Process. *Solid State Commun.* **2006**, *137*, 196–198. [[CrossRef](#)]
25. Irmawati, R.; Nasriah, M.N.N.; Taufiq-Yap, Y.H.; Hamid, S.B.A. Characterization of Bismuth Oxide Catalysts Prepared from Bismuth Trinitrate Pentahydrate: Influence of Bismuth Concentration. *Catal. Today* **2004**, *93–95*, 701–709. [[CrossRef](#)]
26. Zaid, M.; Marwah, A.; Farah, K. Low Temperature Photosynthesis of Bismuth Oxide Nano Powder. *Earth. J. Chem. Sci.* **2019**, *2*, 303–307. [[CrossRef](#)]
27. Shinde, P.V.; Ghule, B.G.; Shaikh, S.F.; Shinde, N.M.; Sangale, S.S.; Jadhav, V.V.; Yoon, S.-Y.; Kim, K.H.; Mane, R.S. Microwave-Assisted Hierarchical Bismuth Oxide Worm-like Nanostructured Films as Room-Temperature Hydrogen Gas Sensors. *J. Alloy. Compd.* **2019**, *802*, 244–251. [[CrossRef](#)]
28. Dong, W.; Zhu, C. Optical Properties of Surface-Modified Bi₂O₃ Nanoparticles. *J. Phys. Chem. Solids* **2003**, *64*, 265–271. [[CrossRef](#)]
29. Shokuhfar, A.; Nasir, K.; Esmaeilrad, A.; Mazinani, V.; Mallahi, M.; Shokuhfar, A.; Vaezi, M.R.; Esmaeilrad, A.; Mazinani, V. Synthesis and Characterization of Bismuth Oxide Nanoparticles via Sol-Gel Method. *Am. J. Eng. Res.* **2014**, *03*, 162–165.
30. Yang, Q.; Li, Y.; Yin, Q.; Wang, P.; Cheng, Y.B. Hydrothermal Synthesis of Bismuth Oxide Needles. *Mater. Lett.* **2002**, *55*, 46–49. [[CrossRef](#)]
31. Sanità, G.; Carrese, B.; Lamberti, A. Nanoparticle Surface Functionalization: How to Improve Biocompatibility and Cellular Internalization. *Front. Mol. Biosci.* **2020**, *7*, 381. [[CrossRef](#)]
32. Szejtli Introduction and General Overview of Cyclodextrin Chemistry. *ChemInform* **2010**, *29*, 1750. [[CrossRef](#)]
33. Liu, L.; Guo, Q.X. The Driving Forces in the Inclusion Complexation of Cyclodextrins. *J. Incl. Phenom.* **2002**, *42*, 1–14. [[CrossRef](#)]
34. Jia, F.; Yang, X.; Li, Z. Synthesis and Application of Colloidal Beta-Cyclodextrin-Decorated Silver Nanoparticles for Rapid Determination of Malachite Green in Environmental Water Using Surface-Enhanced Raman Spectroscopy. *RSC Adv.* **2016**, *6*, 92723–92728. [[CrossRef](#)]
35. Sawant, V.J.; Bamane, S.R. PEG-Beta-Cyclodextrin Functionalized Zinc Oxide Nanoparticles Show Cell Imaging with High Drug Payload and Sustained PH Responsive Delivery of Curcumin in to MCF-7 Cells. *J. Drug Deliv. Sci. Technol.* **2018**, *43*, 397–408. [[CrossRef](#)]
36. Uekama, K.; Hirayama, F.; Irie, T. Cyclodextrin Drug Carrier Systems. *Chem. Rev.* **1998**, *98*, 2045–2076. [[CrossRef](#)] [[PubMed](#)]
37. Takahashi, K. Organic Reactions Mediated by Cyclodextrins. *Chem. Rev.* **1998**, *98*, 2013–2033. [[CrossRef](#)]
38. Easton, C.J.; Lincoln, S.F. Chiral Discrimination by Modified Cyclodextrins. *Chem. Soc. Rev.* **1996**, 163–170. [[CrossRef](#)]
39. Hedges, A.R. Industrial Applications of Cyclodextrins. *Chem. Rev.* **1998**, *98*, 2035–2044. [[CrossRef](#)]
40. Zempleni, J.; Wijeratne, S.S.K.; Hassan, Y.I. Biotin. *BioFactors* **2009**, *35*, 36–46. [[CrossRef](#)]
41. González, M.; Bagatolli, L.A.; Echabe, I.; Arrondo, J.L.R.; Argaraña, C.E.; Cantor, C.R.; Fidelio, G.D. Interaction of Biotin with Streptavidin. Thermostability and Conformational Changes upon Binding. *J. Biol. Chem.* **1997**, *272*, 11288–11294. [[CrossRef](#)] [[PubMed](#)]
42. Shaikh, J.; Deshmane, S.V.; Purohit, R.N.; Biyani, K.R. Behavioural Study of Cyclodextrin Inclusion Complex on Enhancement of Solubility of Aceclofenac. *Indian Drugs* **2015**, *52*, 19–23. [[CrossRef](#)]

43. Nosrati, H.; Barzegari, P.; Danafar, H.; Kheiri Manjili, H. Biotin-Functionalized Copolymeric PEG-PCL Micelles for in Vivo Tumour-Targeted Delivery of Artemisinin. *Artif. Cells Nanomed. Biotechnol.* **2019**, *47*, 104–114. [[CrossRef](#)] [[PubMed](#)]
44. Sahari, M.A.; Moghimi, H.R.; Hadian, Z.; Barzegar, M.; Mohammadi, A. Improved Physical Stability of Docosahexaenoic Acid and Eicosapentaenoic Acid Encapsulated Using Nanoliposome Containing α -Tocopherol. *Int. J. Food Sci. Technol.* **2016**, *51*, 1075–1086. [[CrossRef](#)]
45. Das, S.; Ng, W.K.; Tan, R.B.H. Are Nanostructured Lipid Carriers (NLCs) Better than Solid Lipid Nanoparticles (SLNs): Development, Characterizations and Comparative Evaluations of Clotrimazole-Loaded SLNs and NLCs. *Eur. J. Pharm. Sci.* **2012**, *47*, 139–151. [[CrossRef](#)]
46. Aslantürk, Ö.S.; Larramendy, M.; Soloneski, S. Genotoxicity—A predictable risk to our actual world. In *In Vitro Cytotoxicity and Cell Viability Assays: Principles, Advantages, and Disadvantages*; 2018; pp. 1–19. [[CrossRef](#)]
47. Ishiyama, M.; Tominaga, H.; Shiga, M.; Sasamoto, K.; Ohkura, Y.; Ueno, K. A Combined Assay of Cell Viability and in Vitro Cytotoxicity with a Highly Water-Soluble Tetrazolium Salt, Neutral Red and Crystal Violet. *Bio. Pharm. Bull.* **1996**, *19*, 1518–1520. [[CrossRef](#)]
48. Mosmann, T. Rapid Colorimetric Assay for Cellular Growth and Survival: Application to Proliferation and Cytotoxicity Assays. *J. Immunol. Methods* **1983**, *65*, 55–63. [[CrossRef](#)]
49. Stone, V.; Johnston, H.; Schins, R.P.F. Development of in Vitro Systems for Nanotoxicology: Methodological Considerations in Vitro Methods for Nanotoxicology Vicki Stone et Al. *Crit. Rev. Toxicol.* **2009**, *39*, 613–626. [[CrossRef](#)]

Disclaimer/Publisher’s Note: The statements, opinions and data contained in all publications are solely those of the individual author(s) and contributor(s) and not of MDPI and/or the editor(s). MDPI and/or the editor(s) disclaim responsibility for any injury to people or property resulting from any ideas, methods, instructions or products referred to in the content.